The Origin of Memory Effects in the Crystallization of Polyamides: Role of Hydrogen Bonding

Xinran Liu, [a,b,#] Yu Wang, [a,c,#] Zefan Wang, [a,b] Dario Cavallo, [d] Alejandro J. Müller, [e,f]

Ping Zhu, [a] Ying Zhao, [a,b] Xia Dong, [a,b*] and Dujin Wang [a,b]

[a] *CAS Key Laboratory of Engineering Plastics, CAS Research/Education Center for Excellence in Molecular Sciences, Institute of Chemistry, Chinese Academy of Sciences, Beijing 100190, China*

[b] *University of Chinese Academy of Sciences, Beijing 100049, China*

[c] *Shenzhen Key Laboratory of Polymer Science and Technology, College of Materials Science and Engineering, Shenzhen University, Shenzhen 518060, China*

[d] *Department of Chemistry and Industrial Chemistry, University of Genova, via Dodecaneso, 31 - 16146 Genova, Italy*

[e] *POLYMAT and Polymer Science and Technology Department, Faculty of Chemistry, University of the Basque Country UPV/EHU, Paseo Manuel de Lardizabal 3, 20018 Donostia-San Sebastián, Spain*

[f] *Ikerbasque, Basque Foundation for Science, Bilbao, Spain*

[#] XR Liu and Y Wang contributed equally to this work.

* Corresponding author: Xia Dong (xiadong@iccas.ac.cn)

ABSTRACT

The effect of hydrogen bonding stability on the memory effects in the crystallization of long chain polyamides have been investigated by the self-nucleation calorimetric technique. Self-nucleation is characterized by three domains in decreasing temperature order: complete melting or *Domain I*, exclusive self-nucleation or *Domain II* and, self-nucleation and annealing or *Domain III*. The memory effect is observed in the high temperature range of *Domain II* (when all crystals are molten, or in *Domain IIa*). In the low temperature range of *Domain II*, crystal remnants act as self-seeds (i.e., *Domain IIb*). The hydrogen bonds between amide groups were detected with FTIR, and a ratio of the content of hydrogen bonded vs. free amide groups could be calculated. The energy needed to break the hydrogen bonds decreases as the self-nucleation temperature (T_s) increases. This means that hydrogen bonds become weaker (and their amount decrease), while the crystalline memory disappears upon crossing from *Domain IIa* to *Domain I*. Comparing the widths of *Domain IIa* in different polyamides, we found for the first time a clear correlation with the relative content of amide groups with respect to methylene groups in the repeat units. In conclusion, we have demonstrated that memory in polyamides is a strong function of hydrogen bonding between chain segments.

Keywords: crystalline memory, long chain polyamides, hydrogen bonding, self-nucleation

1. Introduction

The so called, “memory effect” in the crystallization of polymers has attracted great attention as a unique feature, not commonly exhibited by low molar mass crystalline substances [1-5]. The memory effect refers both to “morphological” and “kinetic” memory of a given crystalline state. In fact, on one hand after a mild melt treatment, the recrystallized superstructure bears some resemblance to the one existing before melting, in particular in relation to the location of crystalline nuclei and the relative orientation of crystallites [6]. On the other hand, the crystallization temperature upon cooling a non-isotropic melt from a relatively low temperature (i.e., when the semi-crystalline polymer is heated to a temperature just above its melting temperature for a short time) increases with respect to that of the isotropic melt (a melt state where the melting temperature is high enough, and the time remaining at that temperature long enough, to erase all memory effects and to produce a random assembly of interpenetrated random coils that are fully relaxed) [7-10].

The classical approach to the study of melt-memory effects in polymer crystallization is the application of the DSC “self-nucleation” protocol proposed by Fillon et. al. [2] and extensively used and reviewed by Müller and co-workers [11-13]. The memory effect in crystallization has been also referred to as self-seeding or self-nucleation [5]. An increase of melting temperature or an extended duration at a specific melting temperature can reduce the re-crystallization rate [3, 12, 14]. However, the above mentioned treatments do not affect the structural characteristics during

recrystallization, e.g., the long period and the lamellar thickness [15-17].

To date, researchers have investigated the crystallization memory effect in both homopolymers and copolymers [5, 9, 14, 18-20]. The memory effects of homopolymers have been widely studied, for instance in isotactic polypropylene (iPP) [12, 14, 21], syndiotactic polypropylene (sPP) [15], polycaprolactone (PCL) [12, 22, 23], and polylactic acid (PLA) [5].

However, the mechanism of the memory effect is still under debate. Lorenzo et al. [12], proposed that self-nuclei originated in the high temperature region within *Domain II* (where no trace of crystal fragments remains) are constituted by regions in the melt with the residual orientation that the chains had in the crystalline state [13]. Luo et al. [24] have postulated that memory effect comes from heterogeneities in the topological constraints and melt entanglements distribution. Muthukumar et al. [25] have established a model where all the metastable states between the isotropic melt and the final semi-crystalline state could be represented together by just one metastable state. In this state the nucleation rate is as a function of the melt temperature. Li et. al. [26] proposed that the memory effect is due to the survival of conformational order inside molten lamellae.

Alamo et. al. [7-9, 24, 27] performed a series of experiments on ethylene random copolymers. They found that these copolymers showed strong memory effects, even above the equilibrium melting point. This unique phenomenon may relate to the partitioning of crystallizable sequences in the process of crystallization. During

subsequent melting, the diffusion of these sequences will be hindered by the chain topology, therefore the transition to a randomized melt state is slowed down remarkably [8, 27]. So, in this situation the memory effect is attributed to the topological constraints in the inter-crystalline region which will affect recrystallization [28].

Rheological techniques have been used to detect differences between isotropic and self-nucleated melts in PP-*ran*-PE random copolymers (with compositions rich in PP) [20]. Even though, differences were not detected between isotropic and self-nucleated melts in the Newtonian viscosity or in the relaxation time, the self-nucleated melt was found to display a clear thermo-rheologically complex behaviour. Instead, the isotropic melt was thermo-rheologically simple. The authors proposed that self-nuclei in PP-*ran*-PE random copolymers were formed by clusters of chains that retained the conformations they had when they were part of the crystals.

Up to now, most of the studied systems are polyolefin or olefin-based copolymers [1, 3, 9, 12, 24, 29-32]. The memory effect of polyamide, polyester and other polymer systems with stronger inter-molecular interaction, such as hydrogen bonding has received less attention. In the case of poly(ε-caprolactone) homopolymers (PCLs), rheology has been capable of differentiating isotropic from self-nucleated melts. Both the zero-shear viscosity and entanglement modulus have significantly higher values for the self-nucleated melt in comparison to the isotropic melt, for three PCL samples with different molecular weights. The PCLs self-nucleated melts are also thermo-rheologically complex in contrast to the thermo-rheologically simple behaviour of

isotropic melts [22, 23].

Recently [23], dielectric experiments have been employed for the first time to study crystalline memory effects in PCL. A decrease of the permittivity value of the self-nucleated melt was detected in comparison with that of the isotropic melt state, hence, a small proportion of dipoles are “restricted” in the self-nucleated melt in comparison with the isotropic melt. The authors postulated that in the high temperature region of the self-nucleation domain (i.e., *Domain IIa*), when no traces of crystals can be found as they are all molten, self-nuclei are made up of regions where molten chains have residual hydrogen bonds that can survive after crystal melting, originating the memory effect detected in PCL. The correlations of the results of rheology, DSC and dielectric permittivity was remarkable [23].

Considering hydrogen bonds, polyamides have similarities with polyesters like PCL. According to the literature mentioned above, one would think rheology and dielectric techniques could be applied to polyamides as well. However, both polyamides and polyesters can undergo a solid state polymerization process when they are held at temperatures above T_g because of the reaction between the end groups in the amorphous regions [33]. A significant difference between polyamides and polyesters is that the equilibrium constant for polyamides is around one hundred times or more larger than that for polyesters, and thus the requirements for removal of by-products of the reaction is much less severe in the first case [34], which means that the polymerization reaction occurs much easier in polyamides. Thus, the process of the polymerization

combined with the possible existence of self-nuclei will give a complicated result by rheology and/or dielectric techniques in the polyamide case. Therefore, those techniques are unsuitable for investigating the memory effect in polyamides.

The amide groups in polyamide, with their ability to form strong hydrogen bonds, make this polymer very different with respect to the commonly investigated polyolefins. Investigation of the memory effect of polyamides should provide insights into the relationship between the polymer crystallization and the molecular structure, i.e., chemical constitution and specific intermolecular interactions. Despite several studies on polyamides [16, 35-39], which mainly focused on the orientation induced memory effect and/or the influence on the recrystallization, the relationship between hydrogen bonding and polyamide memory effect in crystallization in the quiescent state has not been fully elucidated in the literature.

As an extension of our previous works on polyamides (homopolymers and copolymers) [40-46], polyamide 1012 (PA1012) is used as a model polymer in this study. It is a typical AABB-type polyamide with long methylene chain segments between two neighbor amide groups, which is polymerized by a condensation reaction between diacid and diamine. This material is an excellent engineering polyamide with superior physical properties, such as toughness, high elastic modulus, lubrication-free performance, low water absorption and adequate dimensional stability. It is extensively used in industrial fields, e.g., automobile manufacturing, electronic appliances and several commodity markets [35, 47]. PA1012 is formed by a precise number of amide

groups and long aliphatic segments, therefore, it can serve as a model for investigating the role of intermolecular interactions on self-nucleation. The influence of memory effects on the crystallization kinetics and on the latent structure persisting in the melt was investigated at different length scales, employing Differential Scanning Calorimetry (DSC), and Fourier Transform Infrared Spectroscopy (FTIR).

2. Experimental section

2.1. Materials

The Polyamide 1012 (PA1012, -[HN(CH_2)$_{10}$NHCO(CH_2)$_{10}$CO]-) employed here is a commercial grade, supplied by Shandong Guangyin New Materials Co., Ltd. The melt flow index of this material is 16 g/10 min, determined at 235 ^{o}C according to ASTM D1238 (2.16 kg). The results of GPC in chloroform, after sample reaction with trifluoroacetic anhydride are shown in Table S1. Although the PA1012 can only dissolve in chloroform after reaction with trifluoroacetic anhydride, causing a certain difference between the true molar mass and the one measured after trifluoroacetylation, the results in Table S1 can be taken as a valid reference value. PA1012 was synthesized from decamethylene diamine and dodecanedioic acid, whose monomers are produced by a microbiological fermentation method [13, 41]. In the last part of the work, some polyamide samples (PA66, PA610, PA612 and PA1212) with different amide group density, i.e., concentration of amide groups along the chain, were employed for comparison purposes. The information and thermal properties of all the samples can be

found in the supporting information, Table S2. All the polyamides were dried under vacuum at temperatures between 80 and 120 °C for 12 h before the experiments. The detailed drying conditions for the different samples are in Table S3.

2.2.Differential Scanning Calorimetry (DSC)

A differential scanning calorimeter (TA Instrument, Q2000) was employed. It was calibrated with an indium standard. The sample mass employed was approximately 4 mg. Samples were sealed in aluminum pans. A constant flow rate of N_2 was employed during the measurements.

(a) Non-isothermal Crystallization. PA1012 was characterized by a "standard" heating-cooling-heating temperature ramp. The samples were heated to 260 °C, kept in the melt for 5 min, then cooled down to 50 °C, and re-heated to 220 °C. All the heating and cooling ramps were performed at a constant rate of 10 °C /min.

(b) Self-nucleation (SN) protocol. The SN procedure was performed according to the following steps:[2,12] (1) Erasure of previous thermal history by holding the sample in the melt at 260 °C for 5 min. (2) Cooling from 260 to 50 °C at 10 °C/min in order to create a crystalline "standard state" in the sample. (3) Self-nucleation (SN) step, where the sample is heated to a selected temperature (T_s) at 10 °C/min and is kept for 5 min at this T_s temperature. Depending on the temperature the sample will either completely melt (if T_s is too high, *Domain I*), it will only self-nucleate, at intermediate T_s temperatures (in *Domain II*) or it will self-nucleate and anneal (if

the T_s temperature is too low and only causes partial melting, i.e., *Domain III*). (4) Cooling from T_s to 50 °C at a rate of 10 °C/min. During this cooling run, the peak crystallization temperature will be monitored to detect any changes that could indicate an increase in its value due to self-nucleation. (5) Subsequent melting of sample by heating from 50 to 220 °C at a rate of 10 °C/min. The SN process was repeated at different T_s temperatures separated by 1 °C in a wide temperature range that encompasses the entire melting range of the polymer and above (i.e., to include all the SN domains and to determine their boundaries). In particular, the T_s temperature at which the self-nucleation is first observed (*Domain I/Domain II* boundary) and the T_s at which the unmelted crystals undergo both annealing and self-nucleation (*Domain II/Domain III* boundary) must be carefully detected [2, 11]. The detailed self-nucleation (SN) procedure is schematically reported in Figure 1a.

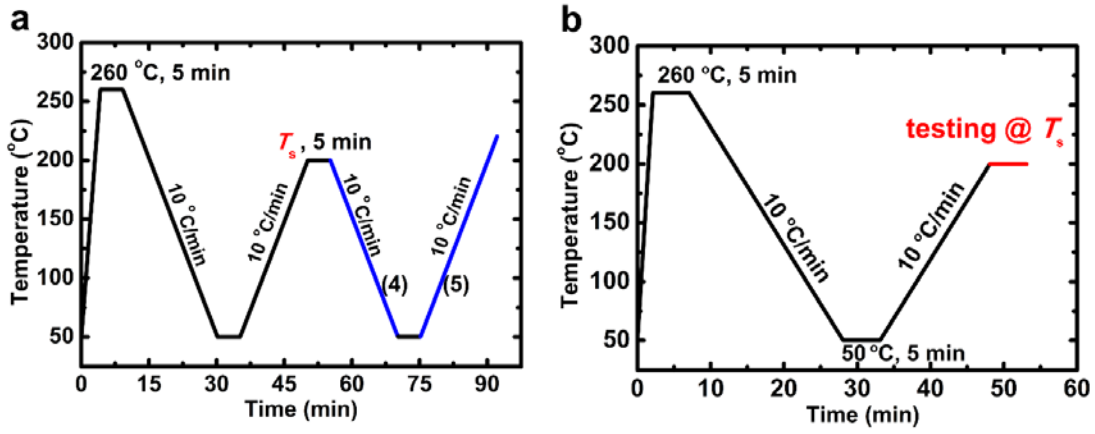

Figure 1. The thermal protocols adopted for self-nucleation experiments employing DSC (a) and *in-situ* FTIR tests (b).

2.3.Fourier Transform Infrared Spectroscopy (FTIR)

FTIR spectra were collected using a Nicolet 6700 Spectrometer (Thermo Fisher Scientific) in transmission mode, with an MCT detector. The spectra were measured with a resolution of 4 cm^{-1} and accumulating 16 scans. The samples were films with 20 μm thickness sandwiched in between potassium bromide thin slices and mounted onto a Linkam FTIR 600 hot stage fitted in the test chamber of the FTIR to record *in-situ* spectra. Temperature calibration of the hot stage was performed with indium and tin standards. The thermal protocol was the same as that applied for the X-ray experiments (Figure 1b). In order to get the conformational information of the PA1012 film at each T_s, the *in-situ* FTIR data were recorded every 30 s while holding the sample at T_s.

3. Results and discussion

3.1. Melt temperature regions at which memory effects can be observed.

The self-nucleation of PA1012 was studied according to the thermal protocol described in Figure 1a. Selected DSC curves recorded during cooling from the indicated T_s temperatures and also during the subsequent heating scans are shown in Figure 2. From the DSC scans presented in Figure 2, the SN domains can be easily obtained [2, 11].

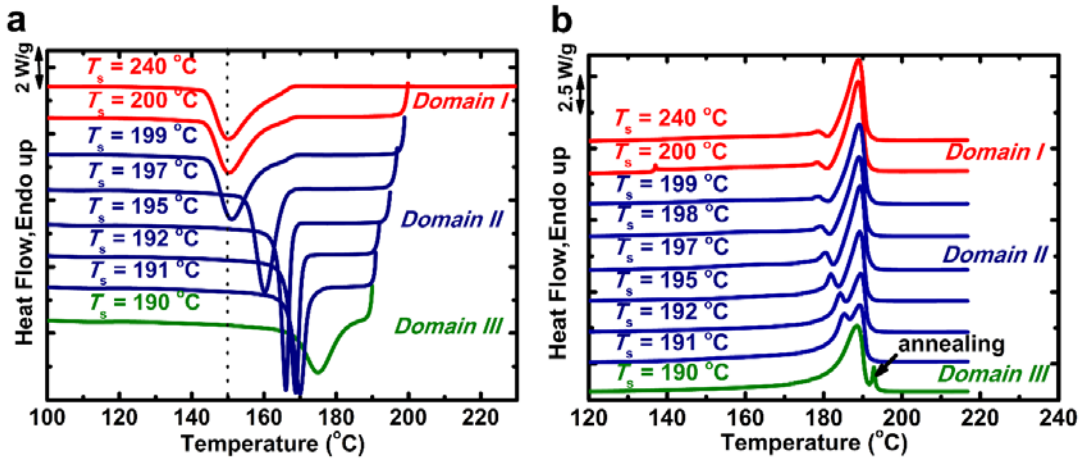

Figure 2. DSC cooling (a) and heating (b) scans of PA1012 after self-nucleation at the indicated T_s.

The memory effect of previous crystalline structure is erased when PA1012 is heated above 199 °C. For this temperature range, the melt is in *Domain I* and the peak crystallization temperature is approximately 150 °C and does not change when the T_s is further increased, as the nucleation density remains constant.

For temperatures lower than 200 °C, but higher than 190 °C, the sample is in the self-nucleation domain, or *Domain II*. The nucleation density is exponentially increased as the T_s temperature decreases, as a result of the large number of self-nuclei produced by the SN thermal protocol [2, 11]. The peak crystallization temperature increases 20 °C with respect to that in *Domain I*.

When the self-nucleation temperature (T_s) is equal to 190 °C or lower, the sample is in the self-nucleation and annealing domain or *Domain III*. The DSC heating scan in Figure 2b for a T_s of 190 °C shows that a new melting endotherm develops: it is a sharp but small second melting peak located at higher temperatures. This corresponds to the

melting of a small crystal population that was not molten at 190 ºC, and had time to anneal during the 5 min waiting period at that temperature (i.e., the crystalline lamellae thickened at 190 ºC and therefore melt at temperatures higher than 190 ºC). This T_s of 190 ºC represents the upper temperature boundary of *Domain III*.

In Figure 3, the recorded peak crystallization temperatures are represented as a function of employed self-nucleation temperatures, and compared with the "standard" DSC melting curve of PA1012. In this way, it is possible to derive the location of the domain boundaries with respect to the melting range of the preexisting crystals.

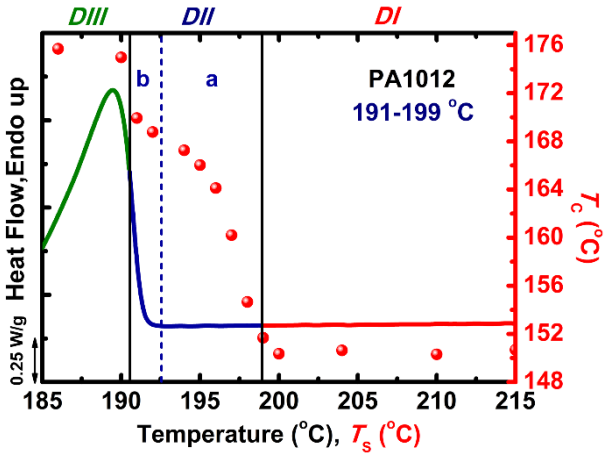

Figure 3. The self-nucleation domains (vertical lines indicate the limits between domains and a color code in the DSC trace has also been employed to differentiate the domains: red for *Domain I*, blue for *Domain II* and green for *Domain III*) for PA1012 represented on the standard DSC melting trace. Data points represent the crystallization temperature peaks (plotted using the right-hand y-axis) as a function of T_s values (on the x-axis). The dotted vertical line divides the *Domain II* into two regions: the higher temperature region "*Domain IIa*" and the lower temperature region "*Domain IIb*".

It can be seen that the boundary between the *Domain III* and *Domain II* is located slightly within the high-temperature tail of the standard melting endotherm. The end of the melting peak is about 2 ºC higher than the boundary temperature between *Domain III* and *Domain II*.

Müller et al. [11, 23] have proposed that *Domain II* should be divided into two regions. The region starting at temperatures higher than the end of the melting endotherm is "*Domain IIa*", or memory effect domain, where all crystals have melted, but the melt still shows a crystalline memory behavior. This self-nucleated melt is not isotropic, thereby producing self-nucleation upon cooling from that T_s temperature range (i.e., upper temperature region of *Domain II*, or *Domain IIa*). The nature of the self-nuclei in *Domain IIa* is unknown for PA1012, and finding out their constitution is one of the aims in this work.

The lower temperature region of *Domain II* is defined as "*Domain IIb*" or "self-seeding domain" [11, 23]. In *Domain IIb*, small crystal fragments remain and they act as crystallographically ideal self-seeds (which greatly increase nucleation density upon cooling from the melt). These small crystals fragments do not anneal during the 5 min spent at T_s.

The temperature boundary between *Domain IIa* and *Domain IIb* is about 193 ºC. The width of the self-nucleation *Domain II* in PA1012 is 9 ºC, indicating a moderate temperature window for the existence of self-seeding (*Domain IIb*) plus memory effects (*Domain IIa*), as commonly observed for several homopolymers. For example, the

width of *Domain II* in iPP is about 4 °C [2], while that of PCL is nearly 10 °C, although it can vary depending on the molecular weight and chain topology (linear versus cyclic) [11, 23]. Polymers with an intrinsically high number density of active heterogeneities (such as high density polyethylene) have a very small width of *Domain II* or in some cases *Domain II* is completely absent [11].

Domain IIa or the "memory effect" domain, is the most interesting to study, as this is the temperature region where memory effects cannot be simply explained by remaining crystal fragments. *Domain IIa* in homopolymers such as iPP [12] is nearly nonexistent, while in PA1012 (6.5 °C) and PCL (9.5 °C) [12], it gets much wider and is even wider in PBS (15 °C) [11]. In order to understand the origin of the memory effect in *Domain IIa*, which persists at temperatures higher than the crystals melting point, several techniques were employed to investigate the existence of order in the self-nucleated melt at different length scales.

3.2.Origin of memory effects of crystallization in PA1012

According to the DSC results shown in Figure 2 and Figure 3, a distinct memory effect on crystallization can be observed in the upper temperature range of *Domain II* (*Domain IIa* region) where no crystalline self-seeds remain. Further FTIR experiments were performed to determine the role of intermolecular interaction on the PA1012 memory effects. It is reasonable to speculate that the ordered structure causing memory effects in polyamide may be due to hydrogen bonds [16, 48], although this link is still

controversial in the literature [16, 36, 48]. In the following, the vibration of the N-H group is particularly considered. Although some researchers state that the N-H stretching is not a conformational sensitive mode, since its peak position remains invariant to the change of the crystalline phase [49, 50], and the vibration band of the carbonyl group should be preferred, the latter is not chosen in this research because of its overlap with other vibration modes [50].

The PA1012 FTIR spectrum of the N-H stretching vibration region is shown in Figure 4, and it can be roughly resolved into three components. Two of the absorption bands can be assigned to the hydrogen bonded and free N-H stretching modes, which are marked as ν $(N\text{-}H)_{bond}$ and ν $(N\text{-}H)_{free}$, respectively [50, 51]. While the one at about 3060 cm^{-1} corresponds to the amide B mode. The amide B is the first overtone of the amide II mode, although there is still some controversy on the origin of this band [52].

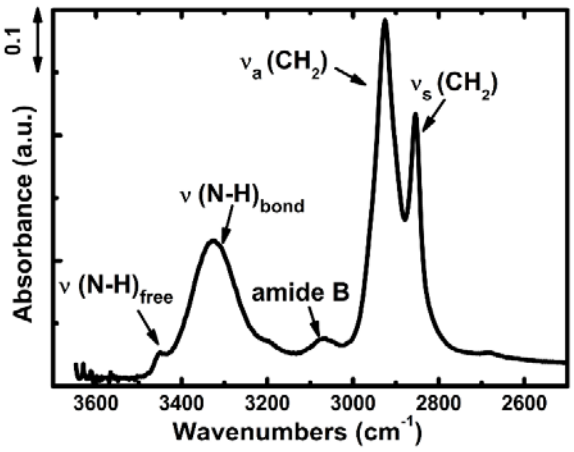

Figure 4. The PA1012 FTIR spectrum of the N-H stretching vibration band.

Curve deconvolution is an accessible way to get more information from the FT-IR

spectra, although some inherent problems exist. Coleman et.al. [53] established criteria for curve fitting of FT-IR spectrum in 1981, and afterwards many other researchers referred to these rules in order to perform curve fitting on FTIR absorption bands. The main issue is to establish band shape, position, width, and the number of curves components comprised in a complex band, as well as the baseline, prior to the fitting process [50]. In this research, the spectra base lines of the N-H stretching region (i.e., from 3120 to 3500 cm^{-1}) have been adjusted separately to obtain a more reliable result. In order to know the number and positions of the curve components in this region, derivative spectroscopy, which has been recognized for many years as a method to enhance the resolution of small shoulders in spectra [53, 54], is applied to the N-H stretching region (Figure S1). As previous researchers report that the frequency difference between the “free” and hydrogen bonded N-H stretching modes is a reflection of the average strength of the hydrogen bonded N-H groups [55], the width of the hydrogen bonded N-H stretching band mainly reflects the distribution of hydrogen bonded groups at different distances and geometries [51, 55]. For the convenience of latter comparisons, and on the basis of the derivative spectra shown in Figure S1, three different peaks have been applied for fitting this wavenumber region. Regarding the employed function for curves fitting, although Gaussian function is very commonly used, the results obtained with this specific peak function are not very satisfactory, especially for sample temperatures of 193 ^{o}C and below (see Figure S2). On the other hand, the Pearson VII function can yield an excellent fit (Figure S3), but

the results lack an exact physical meaning. Therefore, a Gaussian/Lorentz function has been selected as more suitable for approaching the problem of curve fitting, and the results show a very small error. Obeying the above mentioned FTIR fitting rules [53] and using a set of reasonable assumptions, the N-H stretching spectrum, from 3120 to 3500 cm^{-1} after normalization, has been resolved into three bands with the software PeakFit, the outcome for the peak deconvolution is shown in Figure 5 for two representative temperatures.

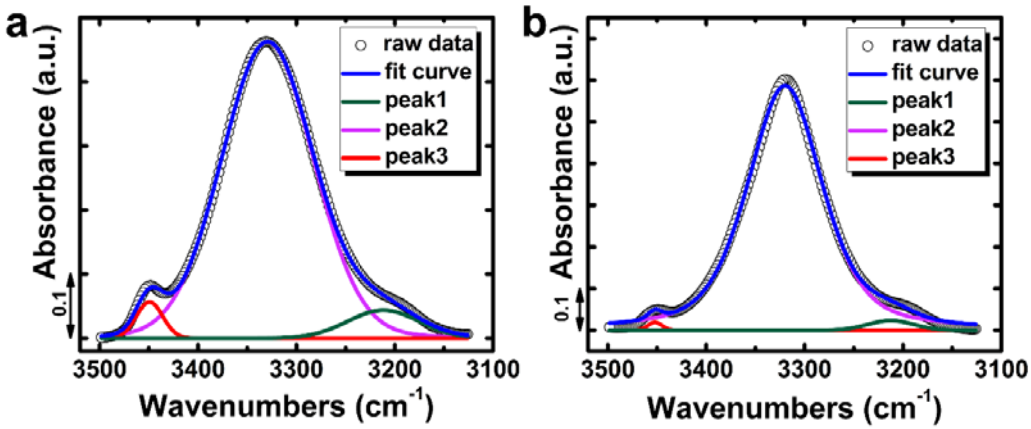

Figure 5. The N-H stretching vibration band peak fitting results at isothermal temperature of 220 °C (a) and 193 °C (b) with Gaussian/Lorentz function.

The data in *Domain I* is fitted with three Gaussian/Lorentz peaks and a good final correlation coefficient is typically obtained. In the lower temperature range of *Domain II*, i.e., 193 °C and below (*Domain IIb*), the fitting results are not perfect, but still acceptable. Considering the second derivative spectra (Figure S1), two small peaks indicated with round blue circles exist at lower temperature especially in *Domain IIb*

and below. The two extra-peaks at 193 °C and below may be originated by the clusters that cause the memory effect, and their presence will have an effect on the fitting quality, if only three fitting peaks are adopted. Nevertheless, despite the lower precision of the fitted curves in that temperature range, we think that the conclusion which are outlined below will not be affected. We must deduce that the state of hydrogen bonded groups in this temperature range is more complicated than that in *Domain I*, as the N-H group in the self-nucleated melt of *Domain II* is possibly experiencing a different vibrational state, or a different degree of bonding dictated by distance and geometry [50]. At a first approximation, the position of the peak is related to the strength of the interaction [50], while the peak height or peak area represents the concentration of the corresponding state. The fraction of each peak obtained by Gaussian/Lorentz fitting after holding at different T_s for 60 min are shown in Figure 6. With the addition of an antioxidant, no detectable degradation has been found during this isothermal process. According to most literature reports [40, 50, 51], we can attribute Peak 2 to the vibration of the hydrogen-bonded N-H groups, while Peak 3, at a higher wavenumber, to that of free N-Hs. Peak 1 is presumably a contribution from a two-phonon band and can be removed by the previously described curve fitting method [51, 55-57].

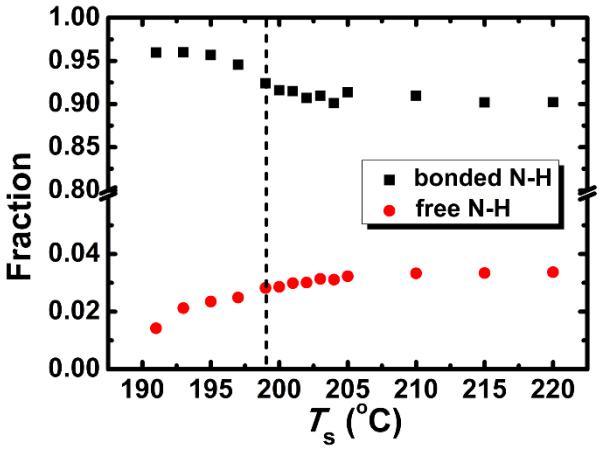

Figure 6. Fraction of the fitted peaks areas as a function of T_s. The boundary temperature between the *Domain I* and *Domain IIa* is indicated by the dashed vertical line.

As shown in Figure 6, the two bands only show significant changes below a T_s values of 200 °C, after which the fractions practically reach a plateau value. Although some researchers [50] claimed that the N-H molar absorption coefficient may vary with the peak position (i.e., wavenumbers), the wavenumber change with temperature of each peak itself was very small compared with the difference in wavenumber between the three peaks. Therefore, we can consider a constant average wavenumber value during the experiment. Besides, a further approximation is to consider the band area proportional to the concentration of the given NH functional group. This choice seems reasonable, given that the relative variation of the absorption band is used in the following calculation.

Under the assumption that all N-H groups in the polymer melt exist in either hydrogen bonded or free state, thus a bonded-free concentration equilibrium for the N-H groups in the system can be established (Equation 1). We highlight that the word

equilibrium is used to indicate an equivalence between the rates of hydrogen bond formation and dissolution, i.e., a kinetically stationary state, rather than a thermodynamic equilibrium. In fact, a continuous conversion between free and bonded N-H groups exists, as it is a dynamic process. On the other hand, the intensity and peak position of the N-H absorption band will not change when the sample is held at T_s for 60 min, so it is deduced that the conversion has reasonably reached a pseudo-equilibrium concentration., and this holding time is employed for FT-IR measurements (Figure S4). Besides, the DSC cooling curves of PA1012, with a standard state, after holding at certain T_s temperature for 5 and 60 min are shown in Figure S5. The crystallization temperature T_c does not change in this time interval. Therefore, the time difference between the DSC and FTIR experiments has no influence on the obtained results. Accordingly, a dynamic equilibrium constant, K_g can be expressed by Equation 2. The equilibrium fraction of bonded N-H, which would possibly be reached after a sufficiently long holding time at T_s, depends on temperature according to Equation 3, where ΔH represents the enthalpy difference between the free and bonded N-H states. As such, taking the area of ν $(N\text{-}H)_{free}$ as the content of $(N\text{-}H)_{free}$, and the areas of the other band as that of the total concentration of $(N\text{-}H)_{bond}$, the equilibrium constant is shown as a function of the inverse of the absolute temperature in Figure 7.

$$(N-H)_{bond} \rightleftharpoons (N-H)_{free} \quad \text{(Eq.1)}$$

$$K_g = \frac{(N-H)_{free}}{(N-H)_{bond}} \quad \text{(Eq.2)}$$

$$\ln K_g = \frac{-\Delta H}{RT} + \frac{\Delta S}{R} \qquad \text{(Eq.3)}$$

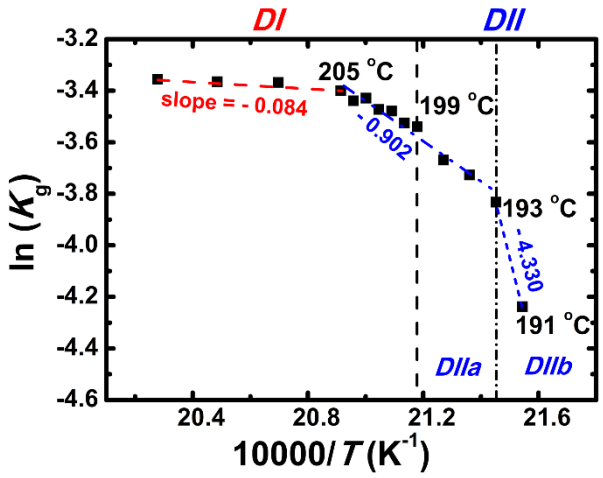

Figure 7. Natural logarithm of the equilibrium constant between hydrogen bonded and free N-H groups as a function of the reciprocal absolute temperature. The dashed vertical lines separate *Domain I* from *Domain IIa* and *Domain IIb*.

Based on the different temperature dependences of K_g in Figure 7, the plot can be clearly divided into three parts. In the higher temperature range of *Domain I* (205 °C and above), the equilibrium ratio of bonded and free N-H is almost constant with the increase of T_s temperature. The temperature dependence of the equilibrium constant K_g becomes stronger when lowering the temperature and it is the strongest for self-nucleation temperatures within *Domain IIb*. From the slope of the plots in the different regions, the corresponding ΔH values are calculated (Table 1). The obtained ΔH represents the average amount of energy that the hydrogen bonded N-H groups, in each identified temperature region, needs to absorb to transform into a free N-H. In other words, it shows that the stabilization of N-H groups by hydrogen bonding is strongest

in *Domain IIb* (about 360 kJ/mol) and is minimal in the high temperature range of *Domain I*, although the presence of weak hydrogen bonds was still detected (7 kJ/mol). The ΔH value in *Domain I* is perfectly in line with those obtained by other researches focusing on hydrogen bonding dynamic equilibrium in high-temperature polyamide melt [50,58], proving that our fitting procedure and the obtained results are reliable. The larger ΔH value in *Domain II* indicates the existence of clusters maintained by the hydrogen bonds, which possess larger dissociation energy. In the low temperature region of *Domain I*, the strength of the hydrogen bond is still substantial, i.e., (75 kJ/mol), a value equal to that in *Domain IIa*, but apparently this does not affect the subsequent recrystallization of the polymer. In fact, although the strength of the hydrogen bonds is still high, the absolute content of the ordered chain aggregates is probably too low, hence no meaningful self-nucleation effect is observed. The hypothesis is confirmed in Figure S4, where the absorbance ratio between $\nu(\text{N-H})_{\text{bond}}$ and $\nu(\text{CH}_2)$ as a function of temperature is shown. Besides, the calculation of equilibrium constant has also been done according to Gaussian and Pearson VII function, and the results are included in the Figure S7, which shows that similar trends.

Table 1. Slope of the logarithm of equilibrium constant versus reciprocal temperature and calculated ΔH for each region.

Domains / Items	high temperature range of *DI*	low temperature range of *DI*	*DIIa*	*DIIb*

Slope×10^4 (K)	-0.084	-0.902	-0.902	-4.330
ΔH (kJ/mol)	7	75	75	360

Since the data collected on PA1012 indicates that hydrogen bonding plays an important role in its crystallization memory behavior, the influence of the amide group density in the repeating units of different polyamides is also investigated. Similar SN experiments were performed on PA66, PA610, PA612, and PA1212, and the different self-nucleation temperature domains are compared to the respective DSC melting endotherms in Figure 8. As expected, with the increase of average methylene sequence length in the repeating unit, the melting temperature of the polyamide drops substantially [59, 60], going from more than 250 °C for PA66 to less than 180 °C for PA1212. In parallel, the temperature range of observed memory effect also noticeably decreases, i.e., the width of *Domain IIa (*and *Domain II)* is the largest for PA66 and it gets narrower with the increase of methylene sequence lengths in the polymer repeating unit.

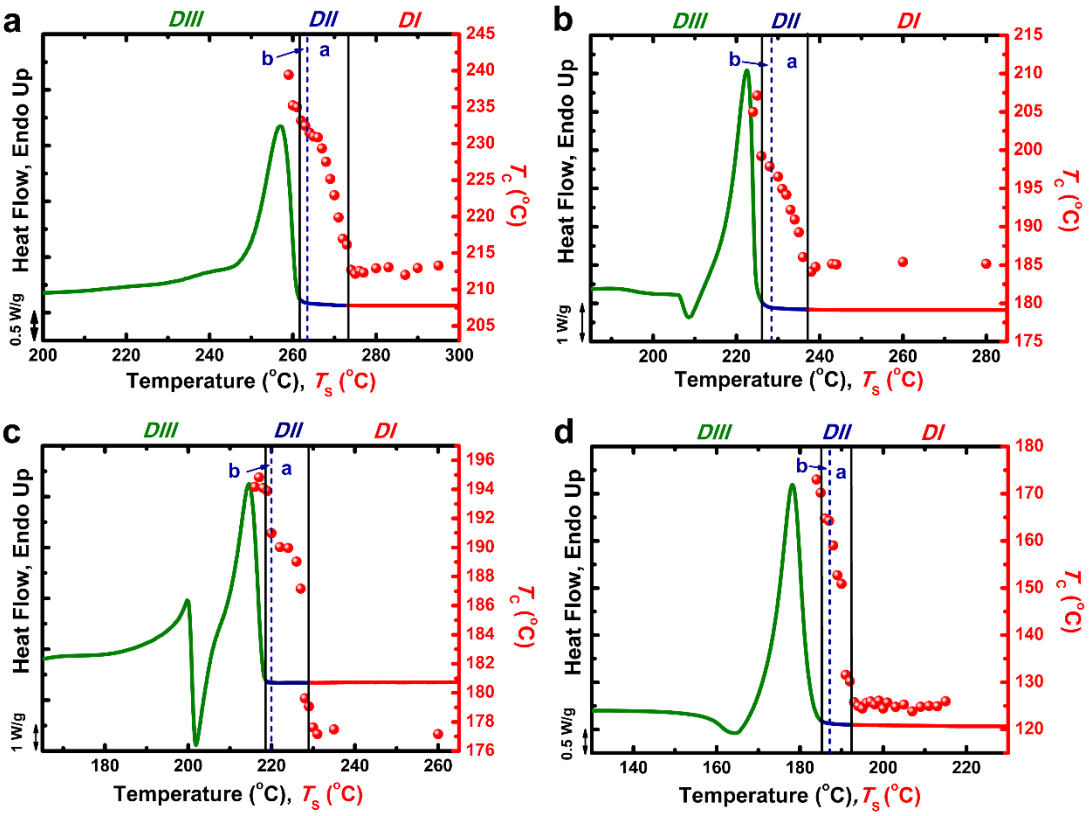

Figure 8. Plots of the self-nucleation domains for PA66 (a), PA610 (b), PA612 (c), and PA1212 (d) homopolymers, overlapped on top of the standard DSC melting traces. Data points represent crystallization temperature peaks (plotted using the right-hand y-axis) as a function of T_s values (on the x-axis).

The widths of *Domain II*, *Domain IIa* and *Domain IIb* temperature ranges are plotted against the ratio of amide groups to methylene groups of each polyamide repeating unit in Figure 9. As deduced from Figure 8, the higher the concentration of hydrogen bonding N-H groups, the higher the stability of the self-nuclei. A very good correlation is found: the width of *Domain II* (and in particular of *Domain IIa*, where no crystalline seeds are present) increases with the increase of the relative contribution of amide group with respect to methylene groups within the chain. On the other hand, the

width of *Domain IIb* is unchanged by the relative content of amide groups. This invariance indicates the predominance of crystalline self-seeds (present as unmelted crystal fragments in *Domain IIb)* as the controlling factor of the memory effect in recrystallization for this temperature region.

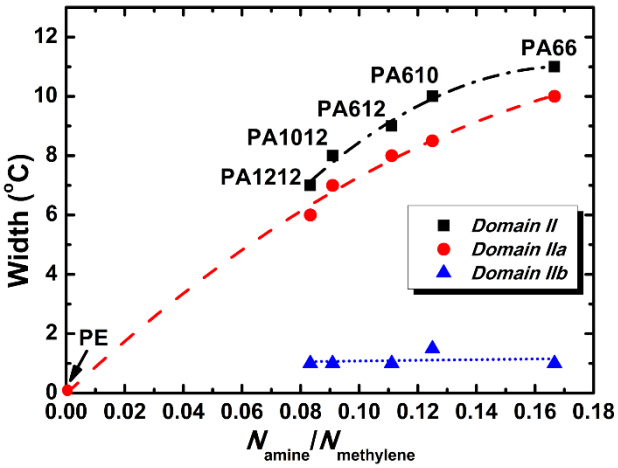

Figure 9. Width of *Domain II*, *Domain IIa* and *Domain IIb* as a function of the ratio of the amide to methylene groups in the repeating units ($N_{amine}/N_{methylene}$) in the different indicated polyamides.

It is remarkable to note that, if the width of *Domain II* (or *Domain IIa*) measured for the different polyamides is extrapolated to a zero amide groups content, a value close to zero is obtained, consistently with the typically negligible width of *Domain II* reported in the literature for linear polyethylene [1, 61, 62]. Therefore, while for polyolefins the origin of intermolecular interactions existing in the self-nuclei [20] needs further investigation, our results demonstrate that in polyamides, when the density of the amide group is high, hydrogen bonding plays a dominating role in the memory effect.

It is conceivable that the strong chain segments interaction through hydrogen bonding slows down the achievement of an isotropic melt after the crystals have disappeared, leading to a persistent memory effect. The higher the relative content of hydrogen bonding groups in the chain repeating units, the higher the thermal energy that should be provided to break these interactions, resulting in a wider *Domain IIa*. This effect might be analogous to the known increase in viscosity and flow activation energy with concentration of hydrogen bonded groups in associative polymers [22].

Despite the limited amount of data for short-chain polyamides in Figure 9, it seems that the width of *Domain IIa* would reach a saturation value at high amide group contents. It can be speculated, that since the hydrogen bonds will make chain segments more rigid, if the length of the methylene chain between the amide groups is very short, the formation of chain aggregates constituting the self-nuclei after the melting of the crystalline structure (see Figure 6) might become more difficult, due to limited chain flexibility.

4. Conclusions

In this work, the crystalline memory of a long chain polyamide, and its relationship with hydrogen bonding, was investigated. FTIR measurements performed during thermal conditioning at different self-nucleation temperatures can successfully detect the presence and stability of hydrogen bonds in the studied polyamide. The variation of the ratio between free N-H and bonded N-H groups can be correlated with the

dependence of the memory effect as a function of T_s values. The results show that the stabilization of N-H groups by hydrogen bonding is strongest in *Domain II* and decreases upon increasing T_s until it becomes significantly smaller in *Domain I*. Employing a series of polyamides, we were able to demonstrate that the width of the memory effect domain (*Domain IIa*) directly correlates with the relative content of amide groups with respect to methylene groups in the repeating units. As such, it was clearly demonstrated that hydrogen bonding plays a fundamental role in the memory effects (observed in *Domain II)* of PA1012, and of long chain polyamides in general. As far as we aware, this is the first time that the key role of hydrogen bonding stability has been unequivocally linked with crystalline memory.

Acknowledgements

This work was financially supported by the National Natural Science Foundation of China (No. 21574140) and the National Key R&D Program of China (No. 2017YFB0307600). The SSRF beamlines BL16B1 are acknowledged for kindly providing the beam time and assistance. We thank Dr. François Bouéfrom CEA UMR12 Lab Léon Brillouin-Orphée Neutron Reactor for the good discussion and help on this work. We also acknowledge funding from the European Union´s Horizon 2020 research and innovation programme under the Marie Sklodowska-Curie grant agreement No. 778092.

Appendix A. Supplementary data

Figure S1-S7, Table S1-S3.

References

[1] W. Banks, M. Gordon, A. Sharples, The Crystallization of Polyethylene after Partial Melting, Polymer 4 (1963) 289-302.

[2] B. Fillon, J.C. Wittmann, B. Lotz, A. Thierry, Self-Nucleation and Recrystallization of Isotactic Polypropylene (α Phase) Investigated by Differential Scanning Calorimetry, J. Polym. Sci., Part B: Polym. Phys. 31 (1993) 1383-1393.

[3] G.C. Alfonso, A. Ziabicki, Memory Effects in Isothermal Crystallization II. Isotactic Polypropylene, Colloid. Polym. Sci. 273 (1995) 317-323.

[4] Y.S. Zhang, L.W. Zhong, S. Yang, D.H. Liang, E.Q. Chen, Memory Effect on Solution Crystallization of High Molecular Weight Poly(ethylene oxide), Polymer 53 (2012) 3621-3628.

[5] H. Zhang, C. Shao, W. Kong, Y. Wang, W. Cao, C. Liu, C. Shen, Memory Effect on the Crystallization Behavior of Poly(lactic acid) Probed by Infrared Spectroscopy, Eur. Polym. J. 91 (2017) 376-385.

[6] J. Xu, Y. Ma, W. Hu, M. Rehahn, G. Reiter, Cloning Polymer Single Crystals through Self-Seeding, Nature Mater. 8 (2009) 348-353.

[7] A. Mamun, X. Chen, R.G. Alamo, Interplay between a Strong Memory Effect of Crystallization and Liquid–Liquid Phase Separation in Melts of Broadly Distributed Ethylene–1-Alkene Copolymers, Macromolecules 47 (2014) 7958-7970.

[8] B.O. Reid, M. Vadlamudi, A. Mamun, H. Janani, H. Gao, W. Hu, R.G. Alamo, Strong Memory Effect of Crystallization above the Equilibrium Melting Point of Random Copolymers, Macromolecules 46 (2013) 6485-6497.

[9] X. Chen, A. Mamun, R.G. Alamo, Effect of Level of Crystallinity on Melt Memory Above the Equilibrium Melting Temperature in a Random Ethylene 1-Butene Copolymer, Mater. Chem. Phys. 216 (2015) 1220-1226.

[10] A. Ziabicki, G.C. Alfonso, Memory Effects in Isothermal Crystallization. I. Theory, Colloid. Polym. Sci. 272 (1994) 1027-1042.

[11] R.M. Michell, A. Mugica, M. Zubitur, A.J. Müller, Self-Nucleation of Crystalline Phases Within Homopolymers, Polymer Blends, Copolymers, and Nanocomposites, Adv. Polym. Sci. 276 (2017) 215-256.

[12] A.T. Lorenzo, M.L. Arnal, J.J. Sánchez, A.J. Müller, Effect of Annealing Time on the Self-Nucleation Behavior of Semicrystalline Polymers, J. Polym. Sci., Part B: Polym. Phys. 44 (2006) 1738-1750.

[13] L. Wang, X. Dong, M. Huang, A.J. Müller, D. Wang, Self-associated Polyamide Alloys with Tailored Polymorphism Transition and Lamellar Thickening for Advanced Mechanical Application, Acs Appl. Mater. Interfaces 9 (2017) 19238-19247.

[14] X. Li, F. Su, Y. Ji, N. Tian, J. Lu, Z. Wang, Z. Qi, L. Li, Influence of the Memory Effect of a Mesomorphic Isotactic Polypropylene Melt on Crystallization Behavior, Soft Matter 9 (2013) 8579-8588.
[15] P. Supaphol, J.S. Lin, Crystalline Memory Effect in Isothermal Crystallization of Syndiotactic Polypropylenes: Effect of Fusion Temperature on Crystallization and Melting Behavior, Polymer 42 (2001) 9617-9626.
[16] J. Kawabata, G. Matsuba, K. Nishida, R. Inoue, T. Kanaya, Melt Memory Effects on Recrystallization of Polyamide 6 Revealed by Depolarized Light Scattering and Small-Angle X-ray Scattering, J. Appl. Polym. Sci. 122 (2011) 1913-1920.
[17] Y. Xu, Y. Wang, T. Xu, J. Zhang, C. Liu, C. Shen, Crystallization Kinetics and Morphology of Partially Melted Poly(lactic acid), Polym. Test. 37 (2014) 179-185.
[18] W. Zhang, Evaluation of the Effect of Melt Memory on Shear-Induced Crystallization of Low-Density Polyethylene, Macromol. Rapid Commun. 27 (2010) 1067-1072.
[19] F.A. And, G.C. Alfonso, Lifetime of Shear-Induced Crystal Nucleation Precursors, Macromolecules 38 (2005) 1723-1728.
[20] L. Sangroniz, D. Cavallo, A. Santamaria, A.J. Müller, R.G. Alamo, Thermorheologically Complex Self-Seeded Melts of Propylene–Ethylene Copolymers, Macromolecules 50 (2017) 642-651.
[21] H. Li, X. Sun, J. Wang, S. Yan, J.M. Schultz, On the Development of Special Positive Isotactic Polypropylene Spherulites, J. Polym. Sci., Part B: Polym. Phys. 44 (2006) 1114-1121.
[22] L. Sangroniz, F. Barbieri, D. Cavallo, A. Santamaria, R.G. Alamo, A.J. Müller, Rheology of Self-Nucleated Poly(ε-caprolactone) Melts, Eur. Polym. J. 99 (2018) 495–503.
[23] L. Sangroniz, R.G. Alamo, D. Cavallo, A. Santamaría, A. Alegría, Differences between Isotropic and Self-Nucleated PCL Melts Detected by Dielectric Experiments, Macromolecules 51 (2018) 3663-3671.
[24] X. Chen, G.D. Wignall, L. He, C. Lopezbarron, R.G. Alamo, SANS Evidence of Liquid–Liquid Phase Separation Leading to Inversion of Crystallization Rate of Broadly Distributed Random Ethylene Copolymers, Macromolecules 50 (2017) 4406-4414.
[25] M. Muthukumar, Communication: Theory of Melt-Memory in Polymer Crystallization, J. Chem. Phys. 145 (2016) 821-614.
[26] X. Li, Z. Ma, F. Su, N. Tian, Y. Ji, J. Lu, Z. Wang, L. Li, New Understanding on the Memory Effect of Crystallized iPP, Chin. J. Polym. Sci. 32 (2014) 1224-1233.
[27] H. Gao, M. Vadlamudi, R.G. Alamo, W. Hu, Monte Carlo Simulations of Strong Memory Effect of Crystallization in Random Copolymers, Macromolecules 46 (2013) 6498-6506.
[28] C. Luo, J.U. Sommer, Frozen Topology: Entanglements Control Nucleation and Crystallization in Polymers, Phys. Rev. Lett. 112 (2014) 195702.
[29] D. Cavallo, F. Azzurri, L. Balzano, S.S. Funari, G.C. Alfonso, Flow Memory and

Stability of Shear-Induced Nucleation Precursors in Isotactic Polypropylene, Macromolecules 43 (2010) 9394-9400.
[30] K. Cho, D.N. Saheb, J. Choi, H. Yang, Real Time in Situ X-ray Diffraction Studies on the Melting Memory Effect in the Crystallization of β-Isotactic Polypropylene, Polymer 43 (2002) 1407-1416.
[31] R. Androsch, B. Wunderlich, Analysis of the Degree of Reversibility of Crystallization and Melting in Poly(ethylene-co-1-octene), Macromolecules 33 (2000) 9076-9089.
[32] A.M. Gohn, A.M. Rhoades, O. David, A. René, Effect of Melt-Memory on the Crystal Polymorphism in Molded Isotactic Polypropylene, Macromol. Mater. Eng. 303 (2018) 1800148.
[33] S.N.Vouyiouka, E.K.Karakatsani, C.D.Papaspyrides, Solid State Polymerization, Prog. Polym. Sci. 30 (2005) 10-37.
[34] Z. Yao, W.H. Ray, Modeling and analysis of new processes for polyester and nylon production, Aiche Journal 47 (2001) 401-412.
[35] L. Chocinski-Arnault, V. Gaudefroy, J.L. Gacougnolle, A. Rivière, Memory Effect and Crystalline Structure in Polyamide 11, J. Polym. Sci., Part B: Polym. Phys. 41 (2002) 777-785.
[36] N. Vasanthan, “Orientation Induced Memory Effect” in Polyamides and the Relationship to Hydrogen Bonding, J. Appl. Polym. Sci. 90 (2003) 772-775.
[37] Y.P. Khanna, R. Kumar, A.C. Reimschuessel, Memory effects in polymers. III. Processing history vs. crystallization rate of nylon 6—comments on the origin of memory effect, Polym. Eng. Sci 28 (1988) 1607-1611.
[38] Y.P. Khanna, A.C. Reimschuessel, Memory effects in polymers. I. Orientational memory in the molten state; its relationship to polymer structure and influence on recrystallization rate and morphology, J. Appl. Polym. Sci. 35 (1988) 2259-2268.
[39] Y.P. Khanna, A.C. Reimschuessel, A. Banerjie, C. Altman, Memory effects in polymers. II. Processing history vs. crystallization rate of nylon 6—observation of phenomenon and product behavior, Polym. Eng. Sci 28 (1988) 1600-1606.
[40] L. Wang, X. Dong, M. Huang, D. Wang, Transient Microstructure in Long Alkane Segment Polyamide: Deformation Mechanism and Its Temperature Dependence, Polymer 97 (2016) 217-225.
[41] L. Wang, X. Dong, X.R. Wang, G.Y. Zhu, H.Q. Li, D.J. Wang, High Performance Long Chain Polyamide/Calcium Silicate Whisker Nanocomposites and the Effective Reinforcement Mechanism, Chin. J. Polym. Sci. 34 (2016) 991-1000.
[42] P. Zhu, X. Dong, Y. Cao, L. Wang, X. Liu, Z. Wang, D. Wang, The Brill Transition in Polyether- b -amide Segmented Copolymers and Composition Dependence, Eur. Polym. J. 93 (2017) 334-346.
[43] P. Zhu, X. Dong, D. Wang, Strain-Induced Crystallization of Segmented Copolymers: Deviation from the Classic Deformation Mechanism, Macromolecules 50 (2017) 3911-3921.
[44] Y. Gao, X. Dong, L. Wang, G. Liu, X. Liu, C. Tuinea-Bobe, B. Whiteside, P. Coates,

D. Wang, C.C. Han, Flow-Induced Crystallization of Long Chain Aliphatic Polyamides under a Complex Flow field: Inverted Anisotropic Structure and Formation Mechanism, Polymer 73 (2015) 91-101.
[45] S. Dong, P. Zhu, J. Liu, D. Wang, X. Dong, Thermal Treatment Effects on the Microstructure and Tensile Properties of Transparent Polyamides, Acta Polym. Sin. 50 (2019) 189-197.
[46] C. Suchocki, R. Molak, Rheological Properties of Polyamide: Experimental Studies and Constitutive Modeling, Chin. J. Polym. Sci. 37 (2019) 178-188.
[47] D. Wang, C. Shao, B. Zhao, L. Bai, X. Wang, T. Yan, J. Li, G. Pan, L. Li, Deformation-Induced Phase Transitions of Polyamide 12 at Different Temperatures: An in Situ Wide-Angle X-ray Scattering Study, Macromolecules 43 (2010) 2406-2412.
[48] M.V. Drongelen, A. Stroeks, G.W.M. Peters, Kinetics of the Deformation Induced Memory Effect in Polyamide-6, Eur. Polym. J. 72 (2015) 296-308.
[49] Y. Wu, Y. Xu, D. Wang, Z. Ying, S. Weng, D. Xu, J. Wu, FT-IR spectroscopic investigation on the interaction between nylon 66 and lithium salts, J. Appl. Polym. Sci. 91 (2004) 2869-2875.
[50] D.J. Skrovanek, S.E. Howe, P.C. Painter, M.M. Coleman, Hydrogen Bonding in Polymers: Infrared Temperature Studies of An Amorphous Polyamide, Macromolecules 18 (1985) 1676-1683.
[51] D.J. Skrovanek, P.C. Painter, M.M. Coleman, Hydrogen Bonding in Polymers. 2. Infrared Studies of Nylon 11, Macromolecules 19 (1986) 699-705.
[52] M. Tsuboi, Some Problems in the Infrared Spectra of Polypeptides and Polynucleotides, Biopolym. Symp. 13 (1964) 527-47.
[53] A. Davis, D.W. Kuehn, M. Starsinic, M.M. Coleman, P.C. Painter, R.W. Snyder, Concerning the Application of FT-IR to the Study of Coal: A Critical Assessment of Band Assignments and the Application of Spectral Analysis Programs, Applied Spectroscopy 35 (1981) 475-485.
[54] W.F. Maddams, The Scope and Limitations of Curve Fitting, Applied Spectroscopy 34 (1980) 245-267.
[55] M.M. Coleman, D.J. Skrovanek, P.C. Painter, Hydrogen Bonding in Polymers: III Further Infrared Temperature Studies of Polyamides, Macromol Symp 5 (2011) 21-33.
[56] W.H. Moore, S. Krimm, Vibrational analysis of peptides, polypeptides, and proteins. II. beta-poly(L-alanine) and beta-poly(L-anaylglycine), Biopolymers 15 (1976) 2439–2464.
[57] M.M. Coleman, M. Sobkowiak, G.J. Pehlert, P.C. Painter, T. Iqbal, Infrared Temperature Studies of a Simple Polyurea, Macromolecular Chemistry & Physics 198 (1997) 117-136.
[58] D. Garcia and H. W. Starkweather, Jr., Hydrogen Bonding in Nylon 66 and Model Compounds. J. Polym. Sci., Polym. Phys. Ed., 23, 557-575 (1985).
[59] N.A. Jones, E.D.T. Atkins, M.J. Hill, S.J. Cooper, L. Franco, Polyamides with a Choice of Structure and Crystal Surface Chemistry. Studies of Chain-Folded Lamellae of Nylons 8 10 and 10 12 and Comparison with the Other 2N 2(N + 1) Nylons 4 6 and

6 8, Macromolecules 30 (1997) 3569-3578.
[60] N.A. Jones, E.D.T. Atkins, M.J. Hill, S.J. Cooper, L. Franco, Chain-folded lamellar crystals of aliphatic polyamides. Investigation of nylons 4 8, 4 10, 4 12, 6 10, 6 12, 6 18 and 8 12, Polymer 38 (1997) 2689-2699.
[61] M. Trujillo, M.L. Arnal, A.J. Müller, E. Laredo, S. Bredeau, D. Bonduel, P. Dubois, Thermal and Morphological Characterization of Nanocomposites Prepared by in-Situ Polymerization of High-Density Polyethylene on Carbon Nanotubes, Macromolecules 40 (2007) 6268-6276.
[62] M. Trujillo, M.L. Arnal, A.J. Müller, S. Bredeau, D. Bonduel, P. Dubois, I.W. Hamley, V. Castelletto, Thermal Fractionation and Isothermal Crystallization of Polyethylene Nanocomposites Prepared by in Situ Polymerization, Macromolecules 41 (2008) 2087-2095.